CHEMISTRY OF MATERIALS
Article

Chem. Mater. **2010,** *22,* 755–761 755
DOI:10.1021/cm9013046

Surface- and Structure-Dependent Catalytic Activity of Au Nanoparticles for Oxygen Reduction Reaction†

Youngmin Lee, Aviva Loew, and Shouheng Sun*

Department of Chemistry, Brown University, Providence, Rhode Island 02912

Received May 12, 2009. Revised Manuscript Received June 2, 2009

Polycrystalline Au nanoparticles (NPs) of 3, 6, and 8 nm were synthesized via solution phase reaction of $HAuCl_4 \cdot 3H_2O$ with *tert*-butylamine borane and oleylamine in tetrahydronaphthalene. The sizes of the Au NPs were tuned by varying the reaction temperatures (40−3 °C). For polycrystalline Au NPs made at room temperature or above, smaller NPs showed more positive onset potential in catalyzing oxygen reduction reaction (ORR) in 0.5 M KOH media. However the most active Au NPs were the 8 nm ones that were synthesized at 3 °C. We rationalized the ORR activity of these Au NPs by the ease of oleylamine surfactant removal and the degree of disorder in the polycrystalline structure. This was further confirmed by the low activity observed from the same Au NPs passivated with hexadecanethiol, or from the Au NPs with higher degree of crystallinity made from the etching of the composite $Au-Fe_3O_4$ NPs.

1. Introduction

Au is considered one of the promising non-Pt fuel cell catalysts as it shows good activity toward oxygen reduction reaction (ORR) in alkaline media.[1−17] In the earlier electrocatalytic studies, bulk single-crystalline Au electrodes were used extensively and (100) planes were found to be more active than other normal crystal planes of (111) or (110).[1−11] This activity difference arises from the fact that HO-Au is formed during the ORR and OH adsorbed on Au (100) plane is more discharged than those on the other planes, which indicates that the intermediate peroxide may be more readily reduced on Au (100), leading to an efficient 4-electron pathway.[1,2] Such crystal plane-dependent catalytic behavior has motivated the study of ORR catalyzed by cubic Au of 40 nm,[15] or even smaller Au nanoparticles (NPs).[16] Although the ORR catalyzed by these Au NPs was found to follow the 4-electron pathway as observed from the bulk Au electrodes, the morphology or crystallinity of these Au NP catalysts were generally not well-defined. Furthermore, Au NPs used for ORR catalytic studies were made in micelle encapsulation with diblock copolymers as surfactant and required a heat treatment procedure to remove the surface polymer coating. Such thermal treatment often causes various degrees of Au NP aggregation or coalescence, deteriorating their catalytic efficiency.

The previous catalytic studies on Au inspired us to study ORR activities of the monodisperse polycrystalline Au NPs. These polycrystalline Au NPs with numerous corners, edges and surface defects might provide more active sites for ORR and allow the reaction to occur at lower overpotentials applied.[18−21] Recently, we prepared polycrystalline Au NPs using simple solution phase synthesis with *tert*-butylamine borane as reducing agent and oleylamine as both reducing agent and stabilizing agent.[22] The 8 nm icosahedral shaped Au NPs have twenty (111) facets and many defects on the surface

† Accepted as part of the 2010 "Materials Chemistry of Energy Conversion Special Issue".

*Corresponding author. E-mail: ssun@brown.edu.

(1) Adzic, R. R.; Strbac, S.; Ananstasijevic, N. *Mater. Chem. Phys.* **1989**, *22*, 349.
(2) Adzic, R. R. Recent Advances in the Kinetics of Oxygen Reduction. In Electrocatalysis; Lipkowski, J., Ross, P. N., Eds.; Wiley-VCH: New York, 1998; p 197.
(3) Adzic, R. R.; Markovic, N. M. *J. Electroanal. Chem.* **1982**, *138*, 443.
(4) Adzic, R. R.; Tripkovic, A. V.; Markovic, N. M. *J. Electroanal. Chem.* **1983**, *150*, 79.
(5) Adzic, R. R.; Markovic, N. M.; Vesovic, V. B. *J. Electroanal. Chem.* **1984**, *165*, 105.
(6) Markovic, N. M.; Adzic, R. R.; Vesovic, V. B. *J. Electroanal. Chem.* **1984**, *165*, 121.
(7) Taylor, E. J.; Vilambi, N. R. K.; Gelb, A. *J. Electrochem. Soc.* **1989**, *136*, 1939.
(8) Strbac, S.; Adzic, R. R. *J. Electroanal. Chem.* **1996**, *403*, 169.
(9) El-Deab, M.; Arihara, K.; Ohsaka, T. *J. Electrochem, Soc.* **2004**, *151*, E213.
(10) Aoun, S. B.; Dursun, Z.; Sotomura, T.; Taniguchi, I. *Electrochem. Commun.* **2004**, *6*, 747.
(11) Kim, J.; Gewirth, A. *J. Phys. Chem. B* **2006**, *110*, 2565.
(12) Luo, J.; Njoki, P. N.; Lin, Y; Wang, L.; Zhong, C. J *Electrochem. Commun.* **2006**, *8*, 581.
(13) Jena, B. K.; Raj, C. R. *J. Phys. Chem. C* **2007**, *111*, 15146.
(14) Hernandez, J.; Solla-Gullon, J.; Herrero, E.; Aldaz, A.; Feliu, J. M. *J. Phys. Chem. B* **2005**, *109*, 12651.
(15) Hernandez, J.; Solla-Gullon, J.; Herrero, E.; Aldaz, A.; Feliu, J. M. *J. Phys. Chem. C* **2007**, *111*, 14078.
(16) Tang, W.; Lin, H.; Kleiman-Shwarsctein, A.; Stucky, G. D.; McFarland, E. *J. Phy. Chem. C* **2008**, *112*, 10515.
(17) Lin, H.; Tang, W.; Kleiman-Shwarsctein; McFarland, E. *J. Electrochem. Soc.* **2008**, *155*, B200.
(18) Mills, G.; Gordon, M. S.; Metiu, H. *J. Chem. Phys.* **2003**, *118*, 4198.
(19) Haruta, M. *Catal. Today* **1997**, *36*, 153.
(20) Campbell, C. *Science* **2004**, *306*, 234.
(21) Lopez, N.; Janssens, T. V. W.; Clausen, B. S.; Xu, Y.; Mavrikakis, M.; Bligaard, T.; Nørskov, J. K. *J. Catal.* **2004**, *223*, 232.
(22) Peng, S.; Lee, Y.; Wang, C.; Yin, H.; Dai, S.; Sun, S. *Nano Res.* **2008**, *1*, 229.

Published on Web 06/24/2009

because of their multiply twinned structures. They are stabilized by oleylamine and are active for CO oxidation at low temperature.[22] Here, we report the electrocatalytic studies of these polycrystalline Au NPs for ORR in alkaline media. We demonstrated that the as-synthesized polycrystalline Au NPs of 3, 6, and 8 nm Au NPs were active even without high temperature annealing or any special surfactant removal treatment. They showed size-dependent ORR activity with smaller NPs or highly disordered Au NPs being more active. This surface and structure dependent activity was further confirmed by the low ORR activity observed from the same Au NPs passivated with hexadecanethiol, or from the Au NPs with higher degree of crystallinity made from the etching of composite Au−Fe_3O_4 NPs.

2. Experimental Section

Chemicals. The following chemicals were used as received: Hydrogen tetrachloroaurate (III) hydrate ($HAuCl_4 \cdot 3H_2O$, Strem Chemicals), *tert*-butylamine borane complex (TBAB, 97%, Sigma-Aldrich), morpholine borane complex (MB, 95%, Sigma-Aldrich), oleylamine (80−90%, Acros Organics), oleic acid (80−90%, Acros Organics), 1,2,3,4-tetrahydronaphthalene (tetralin, 99%, Sigma-Aldrich), 1-octadecene (90%, Sigma-Aldrich), 1-hexadecanethiol (92%, Sigma-Aldrich), potassium hydroxide (Fischer Scientific), Nafion 117 (~5%, Fluka), iron pentacarbonyl ($Fe(CO)_5$, 98%, Sigma-Aldrich).

Synthesis of Au NPs. For a typical synthesis of 6 nm Au NPs, a solution of 10 mL of tetralin, 10 mL of oleylamine, and 0.1 g of $HAuCl_4 \cdot 3H_2O$ was prepared at room temperature (20 °C) and initially stirred for 10 min. 1 mmol of TBAB, 1 mL of tetralin and 1 mL of oleylamine were mixed by sonication and quickly injected into the above solution. (MB, which is a weaker reducing agent, was used for the synthesis of larger Au NPs.) The reaction mixture was further stirred at room temperature for 1 h. Au NPs were precipitated by ethanol addition and collected by centrifugation. The product was redispersed in hexane and separated by ethanol addition and centrifugation. This procedure was repeated 3 times. The final product, 6 nm Au NPs, was dispersed in hexane. Au NP sizes were controlled by varying the TBAB injection temperature (40 °C for 3 nm Au NPs and 3 °C for 8 nm Au NPs).

Synthesis of Au−Fe_3O_4 NPs. 20 milligram of presynthesized 6 nm Au NP seeds in 1 mL of hexane were added to a solution of 20 mL of 1-octadecene with 1 mL of oleic acid and 1 mL of oleylamine. Under a gentle nitrogen flow, the mixture was heated to 120 °C to remove hexane. Under a nitrogen blanket, 0.1 mL of $Fe(CO)_5$ was injected into the solution. The solution was heated to reflux (300 °C) and left at that temperature for 30 min. Afterward, it was cooled to room temperature and exposed to air to form Au−Fe_3O_4 NPs. Isopropanol was added to precipitate the Au−Fe_3O_4 NPs that were collected by centrifugation. The product was redispersed in hexane and separated by adding ethanol and centrifugation. This procedure was repeated three times. The final product, 6−15 nm Au−Fe_3O_4 NPs, was dispersed in hexane.

Etching of Au−Fe_3O_4 NPs. 50% by weight of the Au−Fe_3O_4 NPs on carbon support (40 mg in total) were well-mixed in hexane and then dried with nitrogen. 10 mL of 0.5 M H_2SO_4 was added to the mixture, and the mixture was sonicated for 3 h. Catalysts were separated and washed with deionized water three times. The final product was separated by centrifugation.

Sample Preparation for Electrochemical Measurements. Au NPs were dried under N_2 and deposited on carbon support (Ketjen carbon, surface area 800 m^2/g) by ultrasonification for 2 h in hexane (25 wt % of Au on carbon). The dried catalyst (Au/C) was then prepared in water with the concentration being 2 mg/mL and was sonicated for 1 h. 20 μL of the mixture was added to the glassy carbon working electrode (5 mm in diameter, mirror polished), and water was dried in a vacuum. Afterward, the catalyst was covered with a thin layer of Nafion (0.1% in water, 10 μL). Precise weight percentage of Au in Au−Fe_3O_4 NPs was obtained by dissolving Au−Fe_3O_4 NPs in aqua regia and measuring the Au concentration with inductively coupled plasma−atomic emission spectroscopy (ICP-AES).

Electrochemical Measurements. Electrochemical measurements were performed on a Pine Electrochemical Analyzer, model AFCBP1, by typical cyclic voltammetry technique. Hg/HgO (Koslow, filled with 0.5 M KOH) and Pt wire were used as reference and counter electrodes respectively. The reaction was carried out in 0.5 M KOH solution. The catalyst was cleaned by prescanning in the test solution between −700 mV and 200 mV for 20 cycles under saturated N_2 atmosphere. ORR was monitored by changing the rotation speed from 400−2500 rpm (rotation per minute) under O_2 saturation conditions.

Other Characterizations. Samples for transmission electron microscopy (TEM) analysis were prepared by depositing and drying a single drop of diluted Au NP dispersion in hexane on amorphous carbon coated copper grids under ambient condition. Images were obtained by a Philips EM 420 (120 kV). High resolution transmission electron microscopy (HRTEM) images were obtained on a JEOL 2010 TEM (200 kV). Powder X-ray diffraction (XRD) patterns were obtained on a Bruker AXS D8-Advanced diffractometer with Cu Kα radiation (λ = 1.5418 Å). Energy-dispersive spectroscopy (EDS) was measured by Oxford energy-disperse X-ray spectroscopy.

3. Results and Discussion

Synthesis of Monodisperse Au NPs. Different sizes of monodisperse Au NPs were synthesized by injecting TBAB complex to tetralin solution containing $HAuCl_4 \cdot 3H_2O$ in the presence of oleylamine.[22] The reaction temperature at which the reducing agent TBAB solution was injected was the key for Au NP size control. The injection at 40 °C gave 3 nm Au NPs, at room temperature (20 °C) yielded 6 nm Au NPs, and in ice-bath (3 °C) led to 8 nm Au NPs. After the injection of TBAB, a burst nucleation event occurred as indicated by the immediate color change of the reaction mixture from light orange to dark purple. When the reaction was held in an ice-bath, the nucleation process was slowed down and the color change was observed over 5 min. Because fewer nuclei are formed initially at this low temperature, more Au precursors in the solution were available for Au growth into larger NPs. Figure 1A−C shows the TEM images of the as-synthesized Au NPs with different sizes (3, 6, 8 nm). Figure 1D−F shows HRTEM images of the representative 3, 6, and 8 nm NPs. From HRTEM images, we can see that Au NPs in three different size ranges are not single-crystalline. Instead, they contain various twinned structures. Figure 1E shows a single 8 nm Au NP cross-section

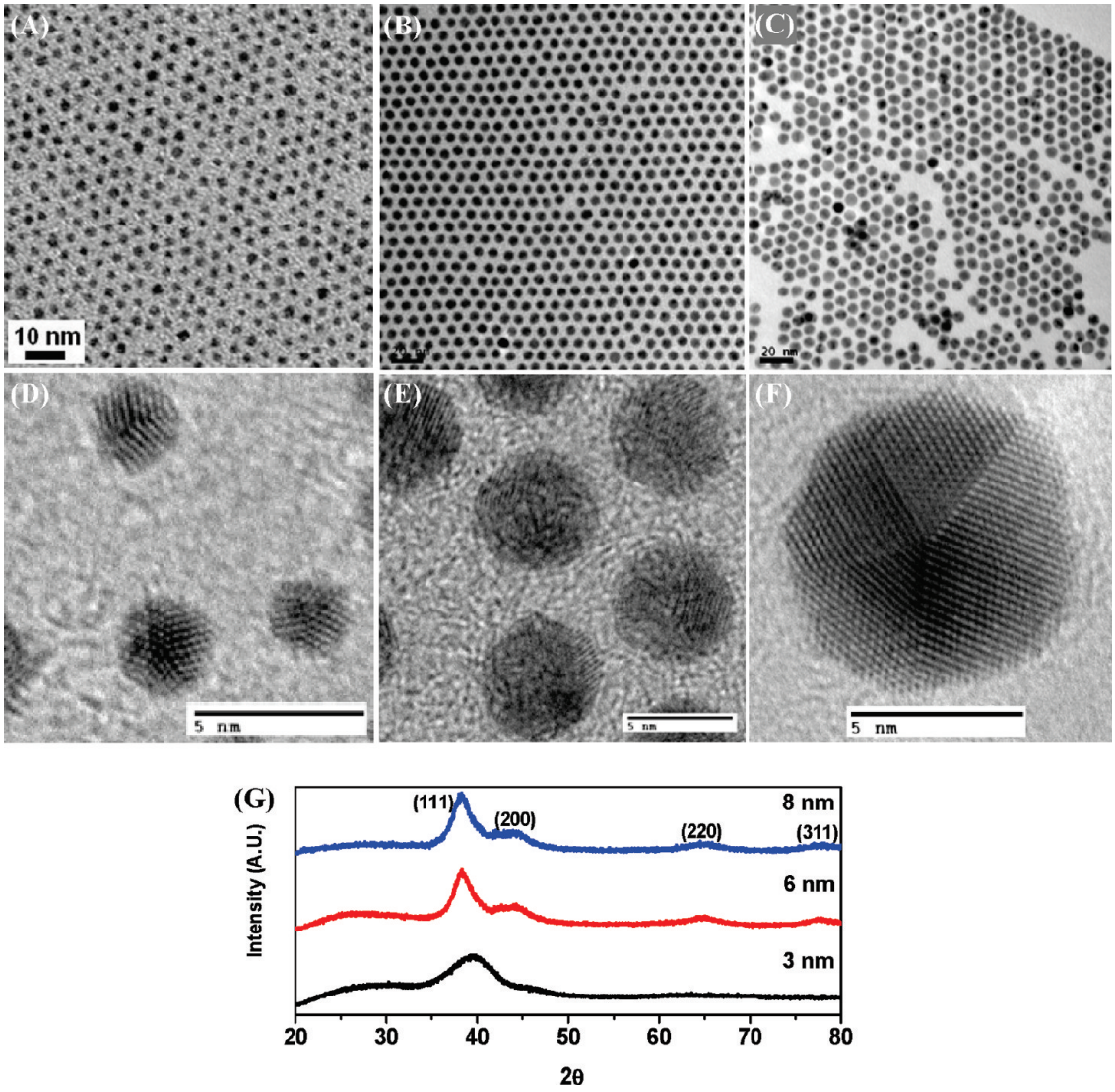

Figure 1. TEM images of the as-synthesized (A) 3, (B) 6, and (C) 8 nm Au NPs; HRTEM images of (D) 3, (E) 6, and (F) 8 nm Au NPs showing polycrystallinity with more well-defined icosahedral structure in the 8 nm Au; (G) XRD patterns of the three different Au NPs.

containing five small single-crystalline domains with (111) facets. It shows a typical 5-fold symmetry of an icosahedral structure, where extra strain/defects are present on the Au NP surface because of the sharing of the twinned planes. XRD patterns of these NPs (Figure 1G) show typical fcc Au diffraction patterns but the peaks are broad and slightly shifted to the right as the particle size decreases. This peak shift may originate from the change in lattice constant due to the strain in the twinned structures. For the 3, 6, and 8 nm Au NPs, the crystal grain sizes estimated from the XRD patterns using Scherrer's equation are 1.77, 3.68, and 3.77 nm respectively. The estimated grain sizes are smaller than those measured from the TEM images, confirming that Au NPs are polycrystalline.

Synthesis of Au−Fe_3O_4 NPs. The polycrystalline Au NPs can be used as seeds to synthesize Au−Fe_3O_4 NPs. The synthetic procedure is similar to what has been reported via thermal decomposition of $Fe(CO)_5$ onto presynthesized Au seeds,[23] but the Au NP seeds here are made from TBAB reduction and are polycrystalline. In the synthesis, $Fe(CO)_5$ was injected into the mixture of the polycrystalline Au seeds with oleylamine and oleic acid in 1-octadecene at 120 °C, and the solution was then heated to 300 °C. As Fe starts to nucleate and grow on one site on an Au seed, the slight electron density change in Au made by Fe nucleation and growth prohibits the multinucleation of Fe on other sites of Au in current reaction conditions, giving only a dumbbell-like structure. Further oxidation of Fe under air yielded Au−Fe_3O_4 NPs. Figure 2A−C shows the TEM images of Au−Fe_3O_4 NPs synthesized by using different sizes of Au seeds shown in Figure 1A−C. Au has higher electron density than Fe_3O_4 resulting in a darker appearance in TEM images. More importantly, the high temperature condition used for nucleation and growth of Fe particles led to further crystallization of Au NPs. A single-crystalline structure of Au is seen in the HRTEM image of a 6−15 nm Au−Fe_3O_4 NP (Figure 2D). This is further

(23) Yu, H.; Chen, M.; Rice, P. M.; Wang, S. X.; White, R. L.; Sun, S. *Nano Lett*. **2005**, *5*, 379.

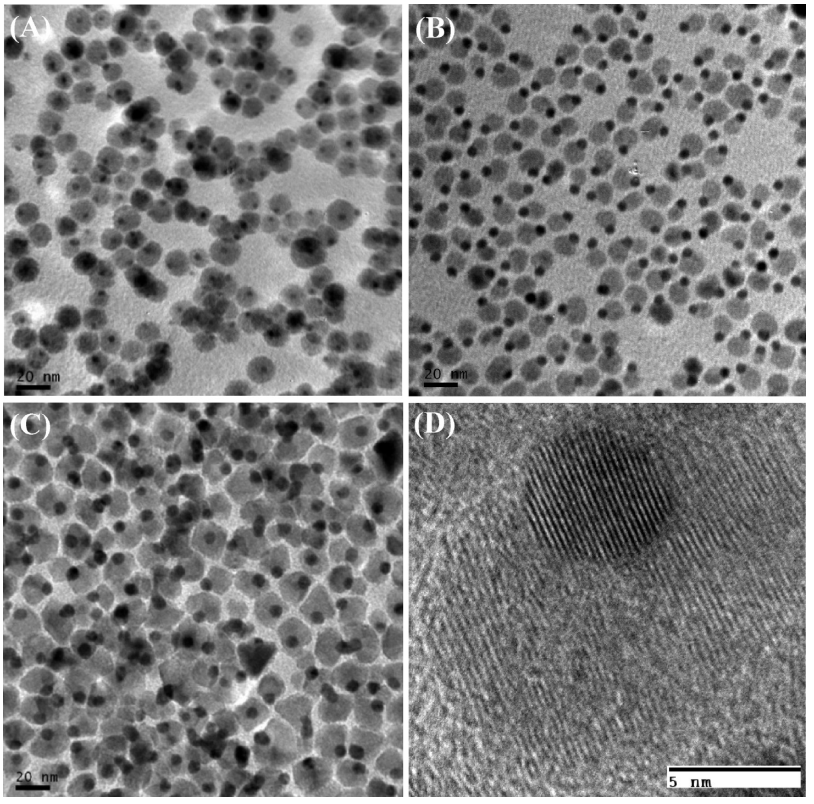

Figure 2. TEM images of (A) 3−17, (B) 6−15, and (C) 8−20 nm Au−Fe_3O_4 NPs; (D) HRTEM image of a 6−15 nm Au−Fe_3O_4 NP showing the single-crystalline Au.

confirmed by XRD patterns of Au−Fe_3O_4 NPs for which the crystal domain size, 5.66 nm, estimated from the Scherrer's equation is similar to that measured from the TEM images.

Catalytic Activity of Au NPs for ORR. The catalytic activity of the polycrystalline Au NPs were studied using electrochemical measurements. Samples of 3 nm (or 6 or 8 nm) Au NPs were deposited on amorphous carbon support to prevent aggregation and to preserve the individual particles during electrocatalytic measurements. The Au/C catalysts were added onto the glassy carbon rotating disk electrode (RDE) as illustrated in the previous section. After water evaporation, the Au/C catalyst was covered with a thin layer of Nafion to ensure that the catalyst adhered to the RDE surface. The RDE was then immersed in 0.5 M KOH solution and ORR measurements were carried out by varying the rotation speed of the RDE under O_2 saturation.

Figure 3A−C shows the TEM images of the 3, 6, and 8 nm Au NPs deposited on carbon support. We can see from the images that the particles are well-dispersed over the support. Typical $I-V$ curves of these Au NPs at various rotation speeds are shown in Figure 3D−F. Commencement of oxygen reduction is indicated by the abrupt increase of current around 0.0 V as potential is applied from positive to negative. All D−F curves show a high degree of saturation at negative potentials, where not much change in current is observed throughout the region, indicating that the $I-V$ curve is dominated by oxygen diffusion process. One important feature of our Au NP catalysts is that it is not necessary to "activate" them by a special treatment as required by most other NP catalysts. Oleylamine is presumably removed during ethanol washing and in the alkaline solution, giving the active Au surface that catalyzes ORR.

To compare the size-dependent catalytic activity, we combined ORR curves at the same rotation speed (1600 rpm) for the 3, 6, and 8 nm Au NPs and 5, and 10 nm commercial Au NPs together in Figure 4. The current is normalized by the weight of Au NPs. We can see that our polycrystalline Au NPs are generally more active than the commercial Au NPs that have larger crystalline domains as shown in the HRTEM image of the representative 10 nm Au NPs (see Figure S1 in the Supporting Information). Among the three polycrystalline Au NPs, the 3 nm Au NPs show better onset potential than the 6 nm Au NPs, which is expected from the smaller size NPs because of the larger number of surface atoms available for oxygen binding.[18−21] However, the 8 nm Au NPs show more positive onset potential than the 3 nm Au NPs. This is likely caused by the low temperature nucleation and growth process during the synthesis of 8 nm Au NPs. At 3 °C, small Au nanocrystallites tend to cluster to form Au NPs, leading to kinetically more favorable well-defined icosahedral structure, as seen in Figure 1F. In this structure, multiply twinned boundaries offer more defects on the NP surface and may provide more active sites for ORR.

ORR studies on bulk single-crystalline Au has indicated that Au atoms on (111) planes are less active than

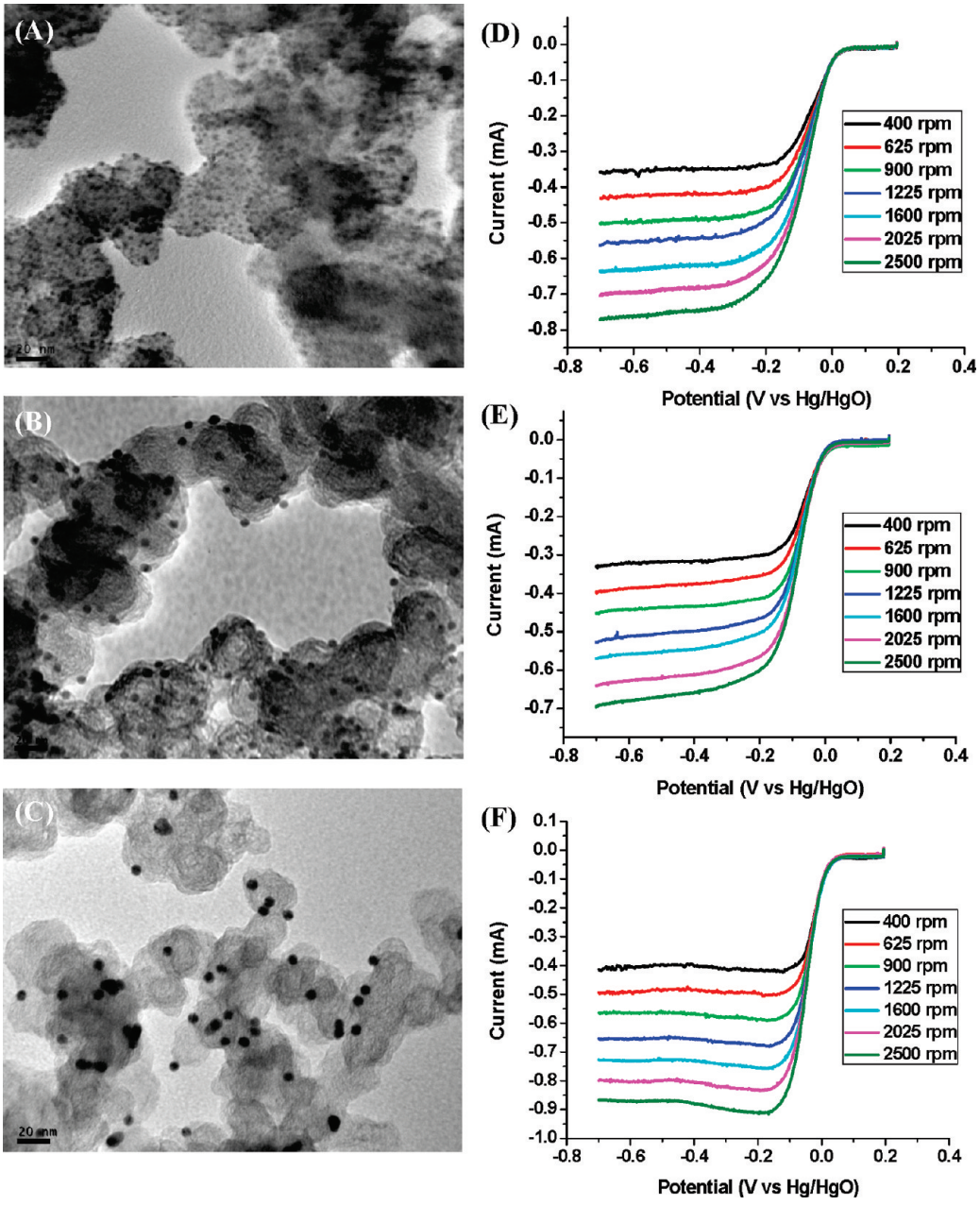

Figure 3. TEM images of (A) 3, (B) 6, and (C) 8 nm Au on carbon support, and (D−F) $I-V$ curves of the A−C catalysts recorded in oxygen saturated 0.5 M KOH as a function of potential at various rotation speeds and a scan rate of 20 mV/s.

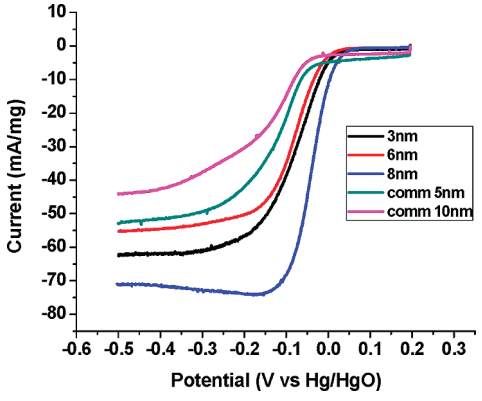

Figure 4. $I-V$ curve of the Au catalysts of both as-synthesized Au NPs and commercial Au NPs recorded in oxygen saturated 0.5 M KOH as a function of potential at a rotation speed of 1600 rpm and a scan rate of 20 mV/s.

those on other crystal planes.[1,12] Generally, ORR on Au can follow either a four-electron process, $O_2 + 2H_2O + 4e^- \rightarrow 4OH^-$, or two two-electron processes $O_2 + H_2O + 2e^- \rightarrow HO_2^- + OH^-$, $HO_2^- + 2e^- + H_2O \rightarrow 3OH^-$ in which the intermediate peroxide ion is further reduced to hydroxide ions. However, the peroxide ion is said to be stable on the Au (111) planes,[1] which hinders the complete reduction of oxygen and a two-electron reduction process is often observed on Au (111). In addition to this, the less favorable O_2 adsorption on the same Au (111), results in low activity of Au (111) compared to other planes in bulk.[1] Nevertheless, our data indicate that even though the Au NPs, especially the 8 nm Au NPs, are composed of numerous {111} facets, they show higher activity. This is likely caused by the presence of the less coordinated Au atoms at the edges and corners on the

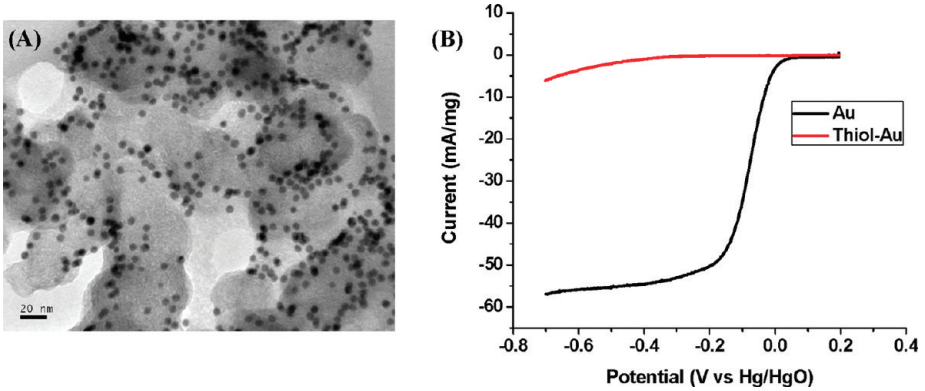

Figure 5. (A) TEM image of the hexadecanethiol treated 6 nm Au NPs on carbon support and (B) $I-V$ curve showing the ORR activity of the as-synthesized 6 nm Au NPs and the thiol treated Au NPs.

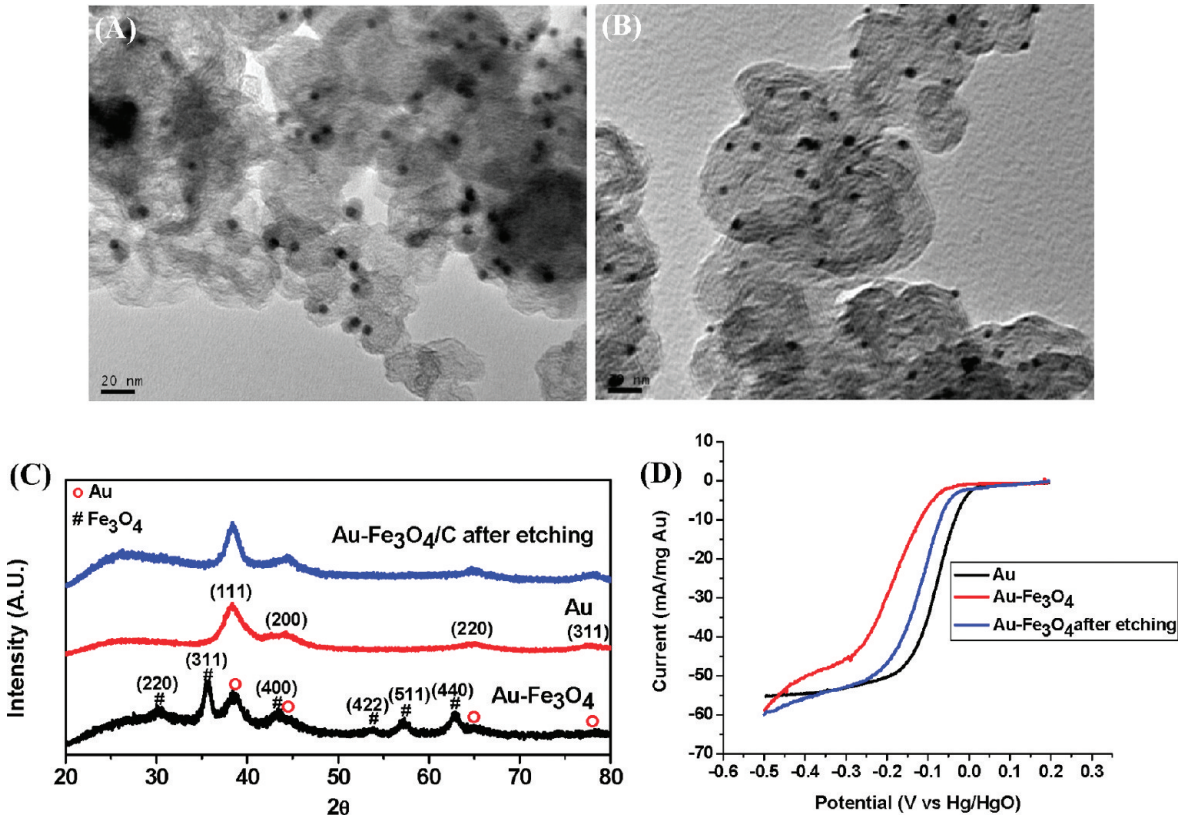

Figure 6. TEM images of (A) 6−15 nm Au−Fe_3O_4 composite NPs on carbon support; (B) 6 nm Au/C after etching Fe_3O_4 from (A); (C) XRD patterns of the original 6 nm Au NPs, 6−15 nm Au−Fe_3O_4 composite NPs made from the same Au seeds, and the 6 nm Au NPs obtained from the Fe_3O_4 etching of Au−Fe_3O_4 NPs on carbon support; (D) $I-V$ curves of the three different Au NPs recorded in oxygen saturated 0.5 M KOH at a rotation speed of 1600 rpm and a scan rate of 20 mV/s.

Au NP surface as the angle of the facets sharing the 5-fold symmetry axis of an icosahedron does not perfectly fit into $72° \times 5 = 360°$; instead each is about 70.5°, leaving a 7.4° gap with extra strain/defects present on the Au NP surface.[24,25] This could explain why our polycrystalline Au NPs have more positive onset potentials compared to both the bulk single crystalline Au (111) at the same condition as reported in literature (see Figure S2 in the Supporting Information), and the commercial Au NPs with larger crystalline domains and less surface defects.

The high activity of the polycrystalline Au NPs further indicates that oleylamine used for Au NP stabilization during the synthesis can be readily removed in the current electrochemical test condition. This is in sharp contrast to the other Au NPs, where stabilizers such as thiol molecules or polymers are often needed for long-term NP protection.[26,27] In these cases, strong bonding between Au and thiol or Au and polymer require high temperature annealing or special surfactant removal treatment to

(24) Wang, Z. L. *J. Phys. Chem. B* **2000**, *104*, 1153.
(25) Marks, L. D. *Rep. Prog. Phys.* **1994**, *57*, 603.
(26) Daniel, M. C.; Astruc, D. *Chem. Rev.* **2004**, *104*, 293346.
(27) Fan, H. Y.; Yang, K.; Boye, D. M.; Sigmon, T.; Malloy, K. J.; Xu, H. F.; Lopez, G. P.; Brinker, C. J. *Science* **2004**, *304*, 567.

obtain clean Au NP surface. Such treatments are often not effective in making catalytically active Au NPs for ORR. In fact, when the surface of our polycrystalline Au NPs was treated with hexadecanethiol, the Au NPs lost their catalytic activity as shown in Figure 5. In this test, Au/C catalyst was immersed in a hexane solution of hexadecanethiol (0.01 mL of hexadecanethiol in 10 mL of hexane) for 30 min, and the catalysts were deposited on the RDE. The treatment did not lead to any morphology change on Au NPs (Figure 5A). The loss in activity of the thiol-exposed Au/C (Figure 5B) further confirms that the catalytic activity of the Au/C comes from the surface of the polycrystalline Au NPs.

Catalytic Activity of Au−Fe_3O_4 NPs and Au NPs Obtained from the Au−Fe_3O_4 NPs. The high-temperature synthesis of Au−Fe_3O_4 NPs converts polycrystalline Au NP seeds into Au NPs with higher degree of crystallinity. Compared with the polycrystalline Au NPs, those in Au−Fe_3O_4 NPs have not only a higher degree of crystal structure but also a junction effect with Fe_3O_4 NPs, which will be discussed later. More interestingly, the Fe_3O_4 unit in Au−Fe_3O_4 can be etched away by an acid, leaving crystalline Au NPs with the NP shape well-preserved. We can now compare catalytic activities of polycrystalline Au NPs, Au−Fe_3O_4 NPs, and crystalline Au NPs.

To perform the tests, we first deposited Au−Fe_3O_4 NPs on carbon support, as illustrated for the sample preparation of polycrystalline Au/C catalyst. Au/C catalyst with higher crystallinity was made by etching Au−Fe_3O_4/C catalyst with 0.5 M H_2SO_4 for 3 h. The successful etching was characterized by TEM, XRD, and EDS (see Figure S3 in the Supporting Information). Figure 6A−B shows TEM images of the Au−Fe_3O_4/C and that after etching. Figure 6C shows the XRD patterns of the polycrystalline Au NPs, Au−Fe_3O_4 NPs, and Au NPs obtained from etching, with Au being 6 nm. It can be seen that the diffraction peaks from the Au in Au−Fe_3O_4 are narrower than the polycrystalline ones, indicating that Au in Au−Fe_3O_4 has higher degree of crystallinity. The $I-V$ curves of ORR from the three different Au NPs are given in Figure 6D. By comparing the onset potentials, we can conclude that polycrystalline Au NPs are the most active catalyst, whereas the Au−Fe_3O_4 are the least active catalyst for ORR. The least active Au in Au−Fe_3O_4 can be attributed to both crystal structure and the Fe_3O_4 junction effects, which make Au electron-deficient as concluded from the previous UV−vis spectrum study.[23] Once Fe_3O_4 is etched away, the junction effect is eliminated and the crystalline Au NPs become more active, but their activity is less than the polycrystalline Au NPs apparently because of their "tidy" surface structure. The 3 and 8 nm Au and their composite Au−Fe_3O_4 NPs show similar trends to 6 nm Au NPs (see Figure S4 in the Supporting Information), confirming that polycrystalline Au NPs are indeed much more active for ORR.

4. Conclusion

In summary, we have reported the synthesis of monodisperse polycrystalline Au nanoparticles and their electrocatalysis for oxygen reduction reaction in alkaline media. 3 and 6 nm Au NPs made from room temperature or above show size-dependent properties, with 3 nm Au NPs being more active in catalyzing oxygen reduction reaction. However the most active Au NPs are the 8 nm ones that are synthesized at 3 °C. This ORR activity is attributed to the ease of oleylamine removal and the degree of disorder on the surface of the polycrystalline structure. This surface- and structure-dependent catalysis is further confirmed by the low activity observed from the same Au NPs passivated with hexadecanethiol, or from the Au NPs with higher degree of crystallinity made from the etching of the composite Au−Fe_3O_4 NPs. The work demonstrates that polycrystalline Au NPs are promising for alkaline fuel cell applications.

Acknowledgment. This work was supported by NSF/DMR 0606264, the Brown seed fund, and a GAANN fellowship (Y.L.). The authors thank Anthony McCormick for his help in acquiring HRTEM images of the Au NPs.

Supporting Information Available: Au NPs characterization and electrocatalysis (PDF). This material is available free of charge via the Internet at http://pubs.acs.org.